Journal of Power Sources 239 (2013) 284–293

Contents lists available at SciVerse ScienceDirect

Journal of Power Sources

journal homepage: www.elsevier.com/locate/jpowsour

Electrical circuit model of a vanadium redox flow battery using extended Kalman filter

M.R. Mohamed*, H. Ahmad, M.N. Abu Seman, S. Razali, M.S. Najib

Sustainable Energy & Power Electronics Research (SuPER) Group, Faculty of Electrical & Electronics Engineering, Universiti Malaysia Pahang, Pekan, Pahang 26600, Malaysia

HIGHLIGHTS

- V-RFB model consists of open-circuit potential, internal resistance n-RC network.
- The parameters obtained from experimental setup and extended Kalman filter (EKF).
- The model accuracy consistent at different pulse voltages at different SOCs.
- The model is validated with experimental charge-discharge characterisation of V-RFB.
- Model presents good accuracy predicting experimental data with minimum error.

ARTICLE INFO

Article history:
Received 9 January 2013
Received in revised form
22 March 2013
Accepted 23 March 2013
Available online 3 April 2013

Keywords:
Vanadium redox flow battery
Electric circuit modeling
Extended Kalman filter
Energy storage

ABSTRACT

This paper presents an equivalent electrical circuit model for a unit cell all-vanadium redox flow battery (V-RFB). The developed V-RFB model consists of an open-circuit cell potential ($E_{cell(ORP)}$) which is in series with an ohmic internal resistance and parallel with an n-Resistor–Capacitor (n-RC) network. The $E_{cell(ORP)}$ represents an intrinsic relationship of the V-RFB state-of-charge (SOC), while the n-RC networks represent the polarization characteristic and dynamic behaviour of the V-RFB. The $E_{cell(ORP)}$ and ohmic resistance parameters are obtained through a direct measurement of an experimental setup of 25 cm^2 unit cell laboratory unit V-RFB, whereas the two pairs of RC network parameters are identified through a recursive algorithm of extended Kalman filter (EKF). The accuracy of this model is verified with different pulse voltages at a few values of SOCs. Ultimately, the model is validated with an experimental charge–discharge characterisation of V-RFB system. Suggestion for system improvement is highlighted.

1. Introduction

Technological advancements have brought very unique opportunities and obstacles. This is also true with energy storage systems where different application demands different attributes of the system, especially with respect to power and capacity ratings [1]. In stationary generation and distribution applications, storage capacity is preferred over performance in order to supply energy to the consumers for longer periods. Conversely, that is not the case in automobile applications, such as electric vehicle, where both power and capacity ratings are highly desired as key parameters in ensuring improved performance and travel mileage.

Unfortunately, such energy storage is rare, albeit all desired features are met; perhaps redox flow batteries (RFBs) can be a viable option in many applications. Sharing the same principle of storing the energy externally as fuel cells, RFB has the advantage of electrically reversing the electrochemical reaction within the cell. Redox flow battery can either be integrated into existing distribution systems or otherwise in a stand-alone mode such as uninterrupted power supply and load levelling devices [2]. With the possibility of rapid charging through electrolyte replacement and its ability to decouple energy and power components, RFB can meet the pulse power requirements of a vehicle. Since the development of RFB in 1970s [3], many types of RFBs have been fabricated and developed including bromide–polysulfide, vanadium–vanadium, vanadium–bromine, iron–chromium, zinc–bromine, zinc–cerium, and soluble lead RFBs. The recent invention is iron–vanadium flow battery which uses mixed Fe/V electrolytes [4,5]. Among others, all-vanadium redox flow battery (V-RFB) offers high energy efficiency, longer operation life and moderate cost. Fig. 1 highlights the development of RFB from 1970s to mid-2000s. The half-cell kinetic reactions are as follows:

* Corresponding author.
E-mail addresses: rusllim@ump.edu.my, rusllim@gmail.com (M.R. Mohamed).

0378-7753/$ – see front matter © 2013 Elsevier B.V. All rights reserved.
http://dx.doi.org/10.1016/j.jpowsour.2013.03.127

Nomenclature

C_{ap}	activation polarization capacitance (transient response)
C_{cp}	concentration polarization capacitance (transient response)
E_{cell}	cell potential; measured across unit cell stack
$E_{cell(ORP)}$	open-circuit cell potential across two electrodes; otherwise abbreviated as $E_{cell(ORP)}$ for Oxidation −reduction redox potential
E_{ap}	activation polarization potential for V-RFB
E_{cp}	concentration polarization potential for V-RFB
E^o	standard electrode potential
EKF	extended Kalman filter
HEV	hybrid electric vehicle
I	applied current during charge and discharge cycle
OCV	open-circuit voltage
P	state estimation covariance
Q	process noise covariance
R	measurement noise covariance
RC	Resistor−Capacitor
R_o	internal ohmic resistance (Ohmic polarization)
R_{ap}	activation polarization resistance (reaction rate loss)
R_{cp}	concentration polarization resistance (mass transport loss)
RFB	redox flow battery
s	seconds
SHE	standard hydrogen electrode
t	time
SOC	state-of-charge
V-RFB	all-vanadium redox flow battery
V(III), V(IV)	vanadium species at different level of oxidation state; V^{3+} and V^{4+} respectively
%	unless mentioned, percentage refers to the completion state of charge or discharge of the battery

Positive electrode

$$VO^{2+} + H_2O \leftrightarrow VO_2{}^{+} + 2H^{+} + e^{-}; \quad E^o = 1.00\ \text{V vs. SHE} \qquad (1)$$

Negative electrode

$$V^{3+} + e^{-} \leftrightarrow V^{2+}; \quad E^o = -0.26\ \text{V vs. SHE} \qquad (2)$$

Note: $VO^{2+} \cong V^{4+}$; $VO_2^{+} \cong V^{5+}$

Being one of the newest types of energy storage, it is clear that this technology is still emerging and has a long way before it can meet the demands of end-users. One important area of development that is still lacking is in system modelling that can assist simulation works in automotive industries, power electronics and control engineering. Even so, latest research interest has grown into the modelling of V-RFB as its technological development has reached the piloted field demonstration stage [6–10].

Trying to predict the behaviour of a complex system can be costly and time-consuming, and modelling can be used to overcome the problem by transforming the complex circuits of the system into more simplified circuits that can be easily analysed. Nevertheless, an accurate model is vital to represent a true description of a natural phenomenon in the system for further analysis of the system. To date, most of existing models for V-RFB [7,11–13] are based on electrochemical model which is more appropriate for describing the dynamic process of chemical reactions occurring on the electrodes within the systems. The model is used in improving the design of the membranes and flow fields, and in determining the optimal operating conditions such as internal reaction, current density and temperature. Nonetheless, such models are not well suited for describing the electrical behaviour of the V-RFB system, which is complex in nature involving partial differential equations and their boundary conditions, as well as highly dependent on the researchers' experience in electrochemical reactions and detailed information of the system. Moreover, an extensive investigation is required as this model requires detailed knowledge of kinetic reactions that takes place in the battery as well as its material properties. Sharkh et al. [14] and Dees et al. [15] suggested that the electrochemical models are best suited for optimization of the physical design aspects of electrodes and electrolytes.

Meanwhile, an equivalent circuit model of V-RFB that represents excellent adaptability and simple realization of a system will aid the design and control of the interfacing electronics, and in the design and analysis of reliability tests. Furthermore, the V-RFB model can be extended to interface with other power electronics devices, which then can be used for both stationary and mobile applications. With the interest growing in automotive industries for reducing hazardous emission, as well as the capability for quick refuelling [16] and flexibility in design [17]; an equivalent electrical circuit of V-RFB will open-up feasibility study opportunities for applications such as hybrid electric vehicle (HEV) as part of the energy storage system [18,19]. Nevertheless, V-RFB exhibits different characteristics compared to other energy storage systems, where it requires different battery management system and control strategies. Hybridising with other types of batteries, as well as performance in

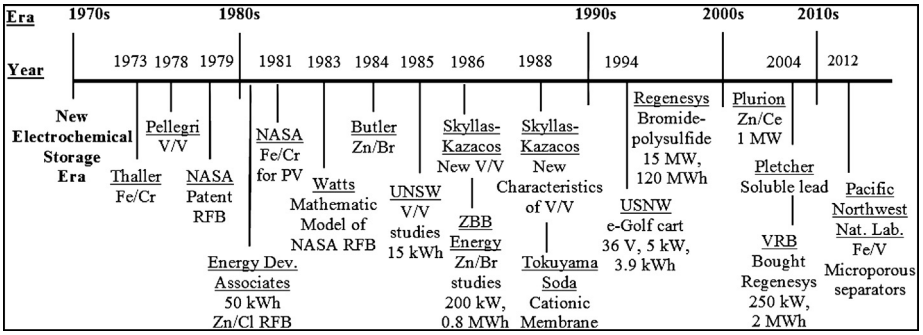

Fig. 1. The development of RFB from 1970s to mid-2000s. Among others, an all-vanadium redox flow battery (V-RFB) has indicated a great potential for many applications. (adapted from Ref. [22]).

propelling power in HEVs, synchronising with grid utility, and control topology for converters to work with V-RFB can be simulated.

Currently, very few publications on studies that have been conducted on the electric circuit model of V-RFB are available. One such study carried out by Chahwan et al. [20] had proposed a simple equivalent circuit for V-RFB, and the model had been analysed and tested by Barote et al. [21] in wind energy simulated systems. Chahwan's [20] investigations were based on estimated losses experienced in the system but no detail explanations were given on how the losses were estimated. Moreover, no comparison was done between the model and other V-RFB characteristics data to prove that the assumed losses made presented a real behaviour of V-RFB system. Nevertheless, the studies offer some parameters of system losses, such as parasitic and pump losses, which needed further investigations. Detail discussion on modelling for V-RFB is covered in Ref. [22].

Meanwhile, based on the assumptions made on the model and depending on a particular application, all techniques used in parameter identification have produced errors. A simple but effective method is to use the linear parameter varying technique that models a battery within a linear region of state-of-charge (SOC). This model represents the battery with a constant function of state-of-charge and temperature, but suffers inherent transitional discontinuity; subsequently noise-free measurement data are required [18]. Another method that can be used to identify the parameters is the spline technique that relies on known data points of polynomials; the higher the degree of polynomials are used, the better the actual system behaviour is emulated, but the issue of overshooting at the intermediate points can still happen. Alternatively, identifying complex relationships between the input and output data sets can be determined using more efficient but non-conventional methods such as artificial neural network (ANN), but sufficient amount of data for training and testing are required in the database. Also, even though the original data are contaminated with noise, the use of extended Kalman filter (EKF) can gauge the states and parameters of the system's dynamic behaviour.

This paper focuses on the identification of an equivalent electrical circuit to represent the dynamic behaviour of the V-RFB system. The combination of EKF and experimental identification methods are used to obtain the circuit model of a unit cell, laboratory unit V-RFB. The aim of the study is to propose an equivalent electrical circuit model of a V-RFB system that is accurate or quasi-accurate, effective and adaptable to any circuitry analysis and design.

2. Model formulation and parameters identification method

2.1. Modelling the battery

A simple equivalent electrical circuit model of the battery consists of an ideal voltage source in series with an internal resistance. Since this circuit does not take into account the true internal resistance of the battery that is highly dependent on the state of charge and the electrolyte concentration, it is only suitable for applications where the state of charge is not important [23]. An improved equivalent circuit model that takes into account of the nonlinear parameters of a battery is based on Thevenin model, where the model uses a combination of SOC dependent voltage source, resistors, capacitors and nonlinear elements that represent the dynamics of the battery.

The structure of the proposed equivalent electrical circuit of V-RFB is given in Fig. 2, which resembles the model used for Li-ion and NiMH batteries [24,25]. The equivalent circuit consists of an open-circuit cell potential, $E_{\mathrm{cell(ORP)}}$ that represents the SOC and temperature of the V-RFB, an internal ohmic resistance, R_{o} that corresponds to the effect of current excitation within the cell stack, and a pair of in-series Resistor–Capacitor (RC) networks that represents the time-dependent V-RFB's dynamics of activation polarisations and concentration polarisations.

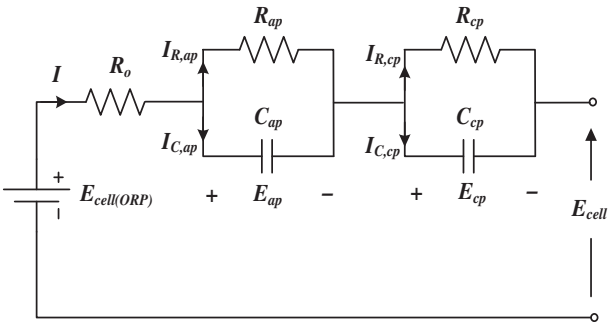

Fig. 2. Equivalent electrical circuit of a unit cell, laboratory unit V-RFB system.

Ideally, for better accuracy and better representation of the complex nonlinear electrochemical processes within the battery, the model must have higher number of RC networks. Nevertheless, at the expense of the complexity of the model as well as insignificant reduction in prediction error of other systems [24,26,27], therefore, Warburg impedance that represents mass transfer diffusion effects is not considered in this model. Furthermore, as the primary aim is to capture the electrochemical trends within the V-RFB by representing in terms of its electrical characteristic, all effects of different operating parameters are excluded. The effects of temperature, flow rate, concentration, and current density that influence the performance of the V-RFB will be considered in a forthcoming paper.

2.2. Modelling equations

Applying Kirchhoff's Voltage Law (KVL) on the V-RFB's equivalent circuit, its electrical behaviour can be expressed as follows:

$$\begin{aligned} &E_{\mathrm{cell}} - E_{\mathrm{cell(ORP)}} - IR_o - E_{\mathrm{ap}} - E_{\mathrm{cp}} = 0 \\ &\therefore E_{\mathrm{cell}} = E_{\mathrm{cell(ORP)}} - IR_o - E_{\mathrm{ap}} - E_{\mathrm{cp}} \end{aligned} \tag{3}$$

Also, applying KVL across the RC networks will result in the following expression:

$$I + I_{R,\mathrm{ap}} + I_{C,\mathrm{ap}} = 0 \tag{4}$$

Substituting $I_{R,\mathrm{ap}} = E_{\mathrm{ap}}/R_{\mathrm{pc}}$ and $I_{C,\mathrm{ap}} = C_{\mathrm{ap}}\mathrm{d}E_{\mathrm{ap}}/\mathrm{d}t$ into (4), the ordinary differential equation across the activation polarization RC network can be expressed as:

$$\dot{E}_{\mathrm{ap}} = \frac{I}{C_{\mathrm{ap}}} - \frac{E_{\mathrm{ap}}}{C_{\mathrm{ap}}R_{\mathrm{ap}}} \tag{5}$$

Since the concentration polarization of the RC network duplicates the activation polarization of the RC network, thus,

$$\dot{E}_{\mathrm{cp}} = \frac{I}{C_{\mathrm{cp}}} - \frac{E_{\mathrm{cp}}}{C_{\mathrm{cp}}R_{\mathrm{cp}}} \tag{6}$$

Taking time-derivative of cell potential, E_{cell} of V-RFB from (1), then,

$$\dot{E}_{\mathrm{cell}} = \dot{E}_{\mathrm{cell(ORP)}} - I\dot{R}_o - \dot{E}_{\mathrm{ap}} - \dot{E}_{\mathrm{cp}} \tag{7}$$

Substituting (5) and (6) into (7), taking into account only the transient response, and assuming the rate of change of $\dot{E}_{\mathrm{cell(ORP)}}$ and $I\dot{R}_o$ against time is negligible, then,

$$\dot{E}_{\text{cell}} = -\left[\frac{1}{C_{\text{ap}}}+\frac{1}{C_{\text{cp}}}\right]I+\left[\frac{1}{C_{\text{ap}}R_{\text{ap}}}\right]E_{\text{ap}}+\left[\frac{1}{C_{\text{cp}}R_{\text{cp}}}\right]E_{\text{cp}} \tag{8}$$

From (1), substituting E_{cp} into (6), thus the state variable of the V-RFB becomes

$$\dot{E}_{\text{cell}} = -\left[\frac{1}{C_{\text{ap}}}+\frac{1}{C_{\text{cp}}}+\frac{R_o}{C_{\text{cp}}R_{\text{cp}}}\right]I+\left[\frac{1}{C_{\text{ap}}R_{\text{ap}}}-\frac{1}{C_{\text{cp}}R_{\text{cp}}}\right]E_{ap} + \left[\frac{1}{C_{\text{cp}}R_{\text{cp}}}\right]E_{\text{cell(ORP)}}-\left[\frac{1}{C_{\text{cp}}R_{\text{cp}}}\right]E_{\text{cell}} \tag{9}$$

2.3. Model parameters identification

Extended Kalman filter (EKF) is a simple, computationally fast recursive algorithm and a very common tool used in estimation problems. Extended Kalman filter makes use of all state space of a model and measured outputs and then recursively approximate the nonlinear model and linearized it into a linear model. The estimation is achieved by minimizing state covariance that reduces the estimation error. The V-RFB's continuous-time model with discrete-time measurements can be illustrated as follows [28]:

$$\begin{aligned} x_k &= f_k(x_{k-1}, u_k, w_k)\\ z_k &= h_k(x_k, v_k)\\ w_k &\sim (0, Q_k)\\ v_k &\sim (0, R_k) \end{aligned} \tag{10}$$

where u_k is the system input current, w_k is the process noise in continuous-time Gaussian zero mean white noise with covariance of Q_k, v_k represents the measurement noise in discrete-time Gaussian zero mean white noise with covariance of R_k. The operation of EKF in estimating optimal- or quasi-optimal value of V-RFB's parameters is illustrated in Fig. 3.

2.4. EKF-based parameters identification for V-RFB

This section focuses on the development of the model by implementing (5), (6) and (9) into state variables for estimating the dynamic parameters of V-RFB in the form of (10) as implemented in Ref. [28].

Let's define the state x_k as:

$$x_k = \begin{bmatrix} E_{\text{ap}} & E_{\text{cp}} & E_{\text{cell}} & \frac{1}{R_{\text{ap}}} & \frac{1}{C_{\text{ap}}} & \frac{1}{R_{\text{cp}}} & \frac{1}{C_{\text{cp}}} \end{bmatrix}^T \tag{11}$$

From the state space model with consideration of the input variable, hence,

$$f(x_k, u_k) = [f_1 \quad f_2 \quad f_3 \quad f_4 \quad f_5 \quad f_6 \quad f_7]^T \tag{12}$$

$$z_k = h_k(x_k) = [0 \quad 0 \quad E_{\text{cell}_k} \quad 0 \quad 0 \quad 0 \quad 0]^T \tag{13}$$

where $u_k = I$, f is transition matrix of V-RFB system, and h_k is measurement matrix. Thus, the f_s are defined as follows:

$$\begin{aligned} &\text{From(5)}, \quad f_1 = -x_1x_4x_5 + x_5u_k\\ &\text{From(6)}, \quad f_2 = -x_2x_6x_7 + x_7u_k\\ &\text{From(9)}, \quad f_3 = -x_3x_6x_7 + x_1(x_4x_5 - x_6x_7)\\ &-(R_ox_6x_7 + x_5 + x_7)u_k + x_6x_7E_{\text{cell(ORP)}}\\ &\text{Thus}, \quad f_4 = f_5 = f_6 = f_7 = 0 \end{aligned} \tag{14}$$

Therefore, from (15), detail matrix representation of the model can be illustrated as:

$$F = \left.\frac{\partial f}{\partial x}\right|_{x=\widehat{x}} = \begin{bmatrix} a_{11} & 0 & 0 & a_{14} & a_{15} & 0 & 0\\ 0 & a_{22} & 0 & 0 & 0 & a_{26} & a_{27}\\ a_{31} & 0 & a_{33} & a_{34} & a_{35} & a_{36} & a_{37}\\ 0 & 0 & 0 & 0 & 0 & 0 & 0\\ 0 & 0 & 0 & 0 & 0 & 0 & 0\\ 0 & 0 & 0 & 0 & 0 & 0 & 0\\ 0 & 0 & 0 & 0 & 0 & 0 & 0 \end{bmatrix} \tag{15}$$

where,

$$\begin{aligned} a_{11} &= -\left(\frac{1}{R_{\text{ap}}C_{\text{ap}}}\right); \quad a_{14} = -\left(\frac{E_{\text{ap}}}{C_{\text{cp}}}\right); \quad a_{15} = -\left(\frac{E_{\text{ap}}}{R_{\text{ap}}}+I\right);\\ a_{22} &= -\left(\frac{1}{R_{\text{cp}}C_{\text{cp}}}\right); a_{26} = -\left(\frac{E_{\text{cp}}}{C_{\text{cp}}}\right); \quad a_{27} = -\left(\frac{E_{\text{cp}}}{R_{\text{cp}}}+I\right);\\ a_{31} &= \left(\frac{1}{R_{\text{ap}}C_{\text{ap}}}\right) - \left(\frac{1}{R_{\text{cp}}C_{\text{cp}}}\right); a_{33} = -\left(\frac{1}{R_{\text{cp}}C_{\text{cp}}}\right);\\ a_{34} &= \left(\frac{E_{\text{ap}}}{C_{\text{ap}}}\right); \quad a_{35} = \left(\frac{E_{\text{ap}}}{R_{\text{ap}}}-I\right);\\ a_{36} &= -\frac{1}{C_{\text{cp}}}\left[E_{\text{cell}} + E_{\text{ap}} + IR_o - E_{\text{cell(ORP)}}\right];\\ a_{37} &= -\frac{1}{R_{\text{cp}}}\left[E_{\text{cell}} + E_{\text{ap}} + IR_o - E_{\text{cell(ORP)}}\right] - I \end{aligned}$$

and the measurement matrix, H as:

$$H = [0 \quad 0 \quad 1 \quad 0 \quad 0 \quad 0 \quad 0] \tag{16}$$

3. Experimental details

Fig. 4 portrays the experimental setup for the study of V-RFB system with concentration flow-tubes, electrical connections, and nitrogen and oxygen flows. The redox couples in V-RFB are all soluble species supplied by Re-Fuel Technology Ltd. with the initial concentration of 1.6 mol dm^{-3} of V(III)/V(IV) in 4 mol dm^{-3} H_2SO_4.

A brief description of the experimental set-up is as follows. The main compartment of the main frame is made up of 10 cm × 10 cm × 4 cm polyvinyl chloride polymer and adopts a flow-through configuration that has a projected electrode area of 5 cm × 5 cm × 0.6 cm Sigratherm GFA5; a porous and layered carbon felt electrodes (effective volumetric porosity of 0.68 ± 0.07) on both positive and negative half-cell. The electrodes are separated by cationic exchange membrane (Du Pont Nafion NF115/H^+). The electrolyte is stored in 250 mL detached-glass reservoir for each half-cell. The electrolyte is circulated through the electrode compartment for each half-cell through Masterflex® Norprene® 06402-25 tube using peristaltic Watson-Marlow 505s pump within nitrogen gas atmosphere, at volumetric flow rate in the range of 3–5 cm^3 s^{-1}, corresponding to linear flow velocity of 1.11–1.85 cm s^{-1}. Pre-written in-house programs in NI LabVIEW 2009 generated all the readings and are then recorded through a 16-Bit, 250 kS s^{-1} isolated M series MIO, bus-powered NI USB-6215 DAQ card. In addition, a 10 A range Fluke 80i-110s AC/DC current probe with an output of 100 mV A^{-1} ±3% (% – accuracy percentage) is used for measuring purposes. Meanwhile, open-circuit cell potential and half-cell redox potentials are monitored using a divided, open-circuit potentiometric cell through a Hach Lange GmbH XR200 Hg/Hg_2SO_4 reference electrode (part no. B20B200) and Sigma–Aldrich 6 mm, 99.9999% (% – weight percentage) graphite rod working electrode (batch no. 11903BB). The cell parameters recorded during the experiment include cell potential E_{cell}, open-circuit cell potential $E_{\text{cell(ORP)}}$, and shunt current I_{shunt}. The variable current load is calibrated in the range of 0.5–5 A,

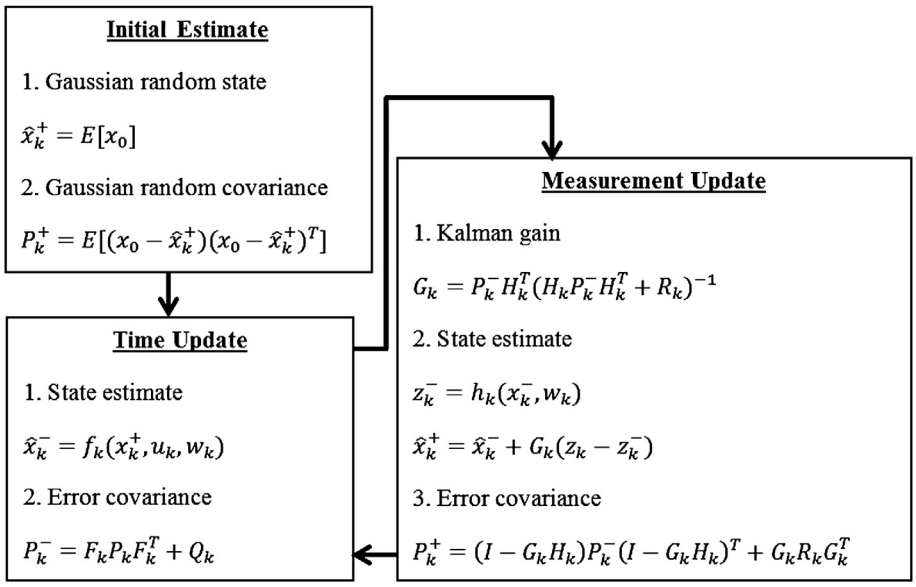

Fig. 3. Operation of EKF in estimating the optimal or quasi-optimal value of V-RFB parameters.

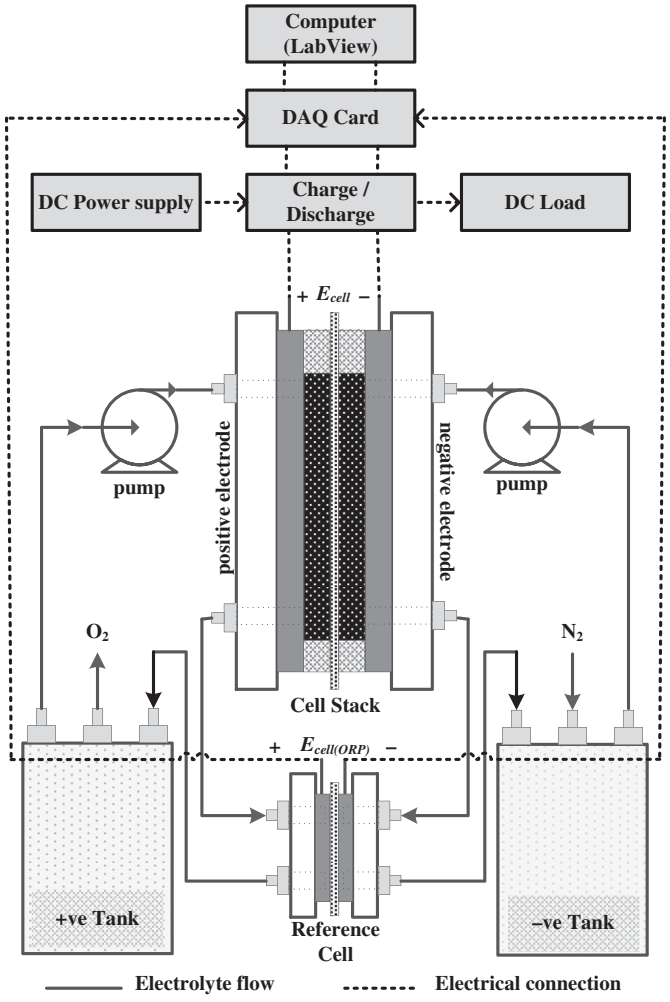

Fig. 4. Configuration of V-RFB test bank with schematic of the overall experimental arrangement including electrolyte flow-tube, nitrogen and oxygen flows, and electrical connection circuits.

corresponding to 20–200 mA cm^{-2} based on the projected area of each electrode, using a Maplins N93CX Switching Mode Power Supply 1.0–20 V_{dc}/0–5A ± 1% (% – accuracy percentage). In addition, the volumetric flow rate and linear flow velocity is calibrated using a Watson-Marlow 505s peristaltic pump with rated rotor speed of 55–220 rpm. Detail explanation of the experimental setup is discussed in Ref. [29].

4. Results and discussions

4.1. Open-circuit voltage and state-of-charge

Open-circuit cell potential, $E_{cell(ORP)}$, also referred as open-circuit voltage (OCV), indicates the equilibrium potential between two electrodes of a cell. Open-circuit voltage can be related directly as a function of SOC; hence accurate estimation of the OCV has led to an accurate estimation of the battery SOC. In this study, the parameter $E_{cell(ORP)}$ is obtained from potentiometric experiment and has been validated by modeling based on Nernst equation and Faraday's law of electrolysis as describe in detail in Ref. [30].

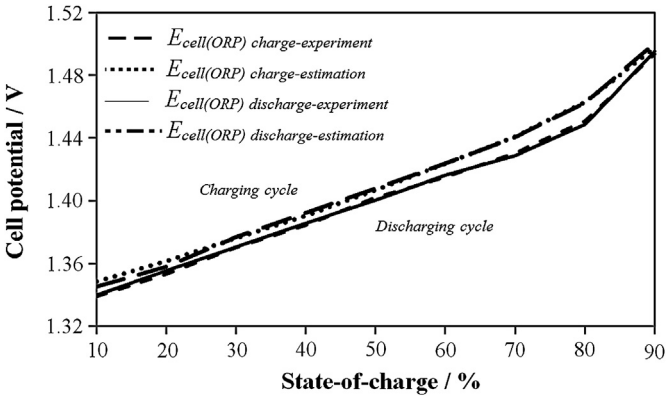

Fig. 5. Open-circuit cell potential $E_{cell(ORP)}$ of a 25 cm^2 unit cell, laboratory unit V-RFB as a function of state-of-charge; comparison of estimated SOC with respect to SOC obtained through experiments for 250 cm^3 (half reservoir) of 1.6 mol dm^{-3} V(III)/V(IV) in 4 mol dm^{-3} H_2SO_4 at linear flow rate of 1.11 cm s^{-1}, constant temperature of 298 ± 2 K and constant current density of 100 mA cm^{-2} (adapted from Ref. [30]).

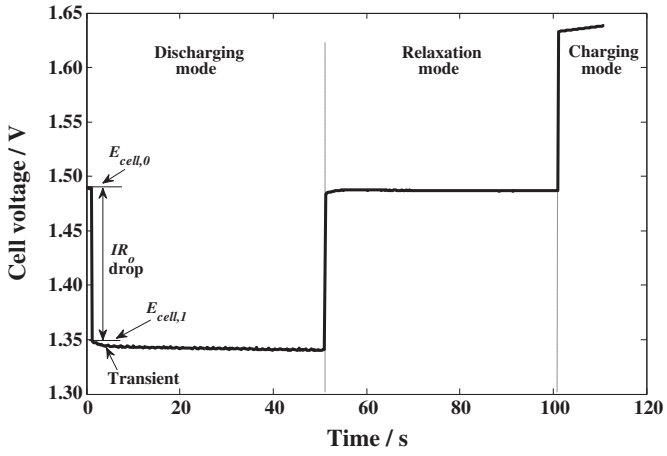

Fig. 6. V-RFB cell voltage characteristic of a 25 cm^2 unit cell, laboratory unit V-RFB during pulse-relaxation test at SOC 80% of 250 cm^3 (half reservoir) of 1.6 mol dm^{-3} V(III)/V(IV) in 4 mol dm^{-3} H_2SO_4, with specific current density of 60 mA cm^{-2}, constant linear flow rate of 1.11 cm s^{-1} and controlled temperature of 298 ± 2 K, simulated through a refrigerated circulators bath (Grant LTD 6/20 − LTD6G).

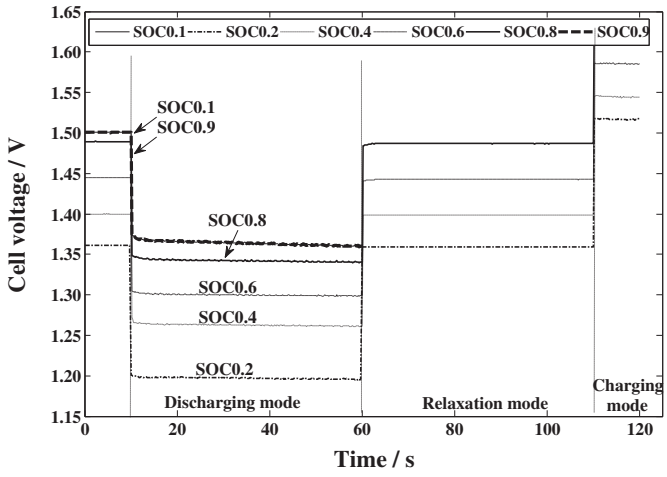

Fig. 7. V-RFB cell voltage characteristic of a 25 cm^2 unit cell, laboratory unit V-RFB during pulse-relaxation test at different SOC from 10% SOC to 90% SOC for 250 cm^3 (half reservoir) of 1.6 mol dm^{-3} V(III)/V(IV) in 4 mol dm^{-3} H_2SO_4 at linear flow rate of 1.11 cm s^{-1}, constant temperature of 298 ± 2 K and current density of at 60 mA cm^{-2}. For simplicity, except 10% and 90% SOC, no odd percentage SOCs are shown.

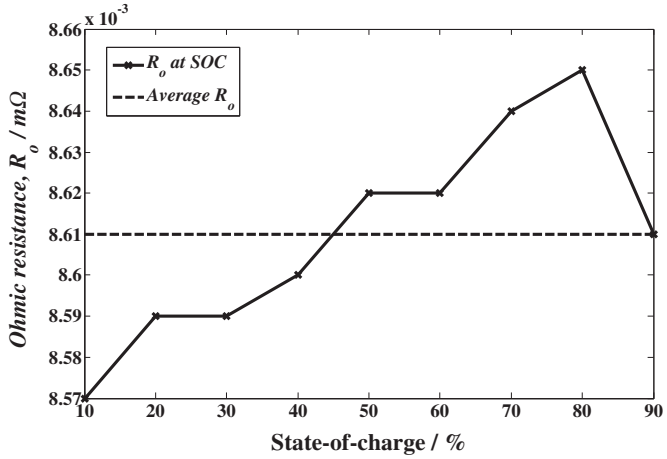

Fig. 8. Ohmic resistance of a 25 cm^2 unit cell, laboratory unit V-RFB at different SOC from 10% SOC to 90% SOC for 250 cm^3 (half reservoir) of 1.6 mol dm^{-3} V(III)/V(IV) in 4 mol dm^{-3} H_2SO_4 at linear flow rate of 1.11 cm s^{-1}, constant temperature of 298 ± 2 K and current density of at 60 mA cm^{-2}.

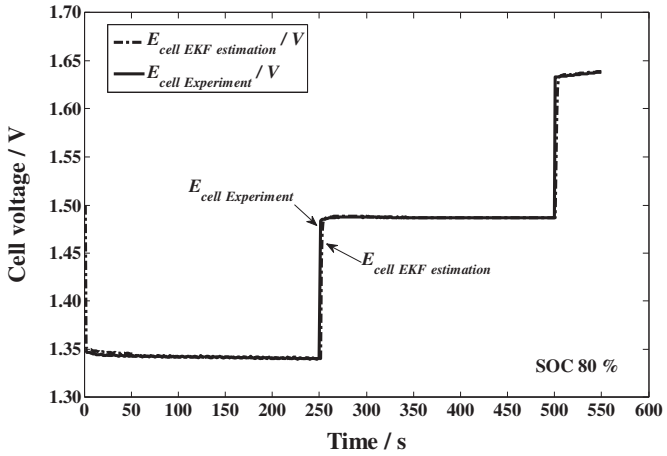

Fig. 9. Comparison of EKF-based estimated E_{cell} and experimental E_{cell} *vs.* time of a 25 cm^2 unit cell, laboratory unit V-RFB during pulse-relaxation test at 80% SOC. Operating parameters are the same as in Fig. 6.

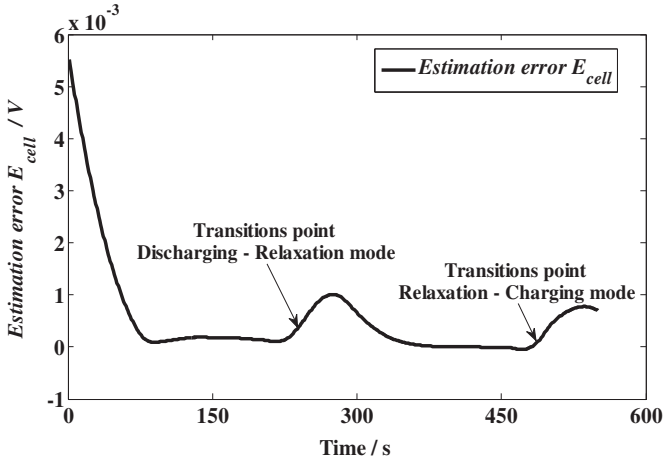

Fig. 10. Estimated error of E_{cell} from the EKF-based estimated with respect to experimental result of pulse-relaxation test at 80% SOC. Operating parameters are the same as in Fig. 6.

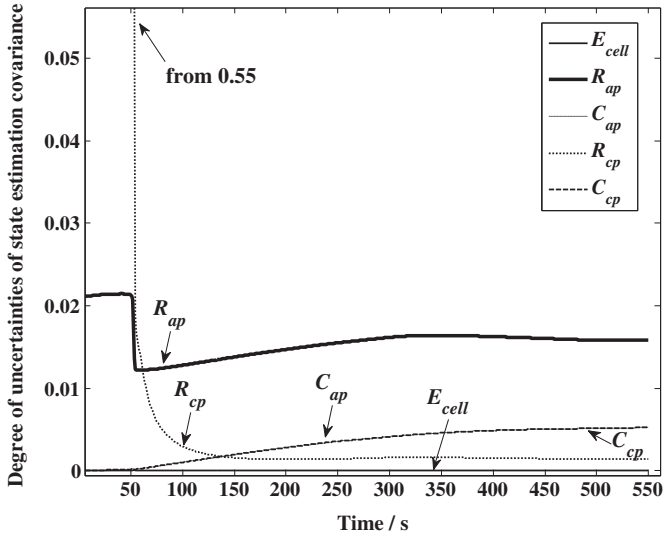

Fig. 11. Degree of uncertainties of the state estimation covariance which depicts all the state estimation smoothly approaching steady state at the end of pulse-relaxation test.

Experimentally, it is observed that $E_{cell(ORP)}$ for 25 cm^2 unit cell, laboratory unit V-RFB delimit to 1.52 V regardless of the applied current densities, up to a maximum of 100 mA cm^{-2}. But, when the OCV is higher than 1.52 V, bubbles are generated and flow into the cell reservoir on the negative side, indicating that side reactions has taken place. Therefore, in this study, $E_{cell(ORP)}$ of the V-RFB cell is charged to a maximum of 1.50 V and discharged to a minimum of 1.34 V. These charging and discharging thresholds, estimated to represent 10–90% SOC, is comparable with the operating region of other reported V-RFB systems [31,32]. The open-circuit cell potential of 25 cm^2 unit cell, laboratory unit V-RFB is presented in Fig. 5.

4.2. Ohmic resistance

Ohmic resistance varies with the voltage level of the battery and is highly dependent on the direction of current flow during the charge and discharge cycles. Meanwhile, one of the common methods used to determine the transient effect of a battery is the pulse-relaxation test [14,18,28,33]. The transient behaviour of the battery can be related to the capacitance of its electrodes, but the voltage drop from relaxation period before the start of the transient mode is directly related to ohmic resistance loss.

Fig. 6 illustrates how ohmic resistance is determined from a pulse-relaxation test for the 25 cm^2 unit cell, laboratory unit V-RFB.

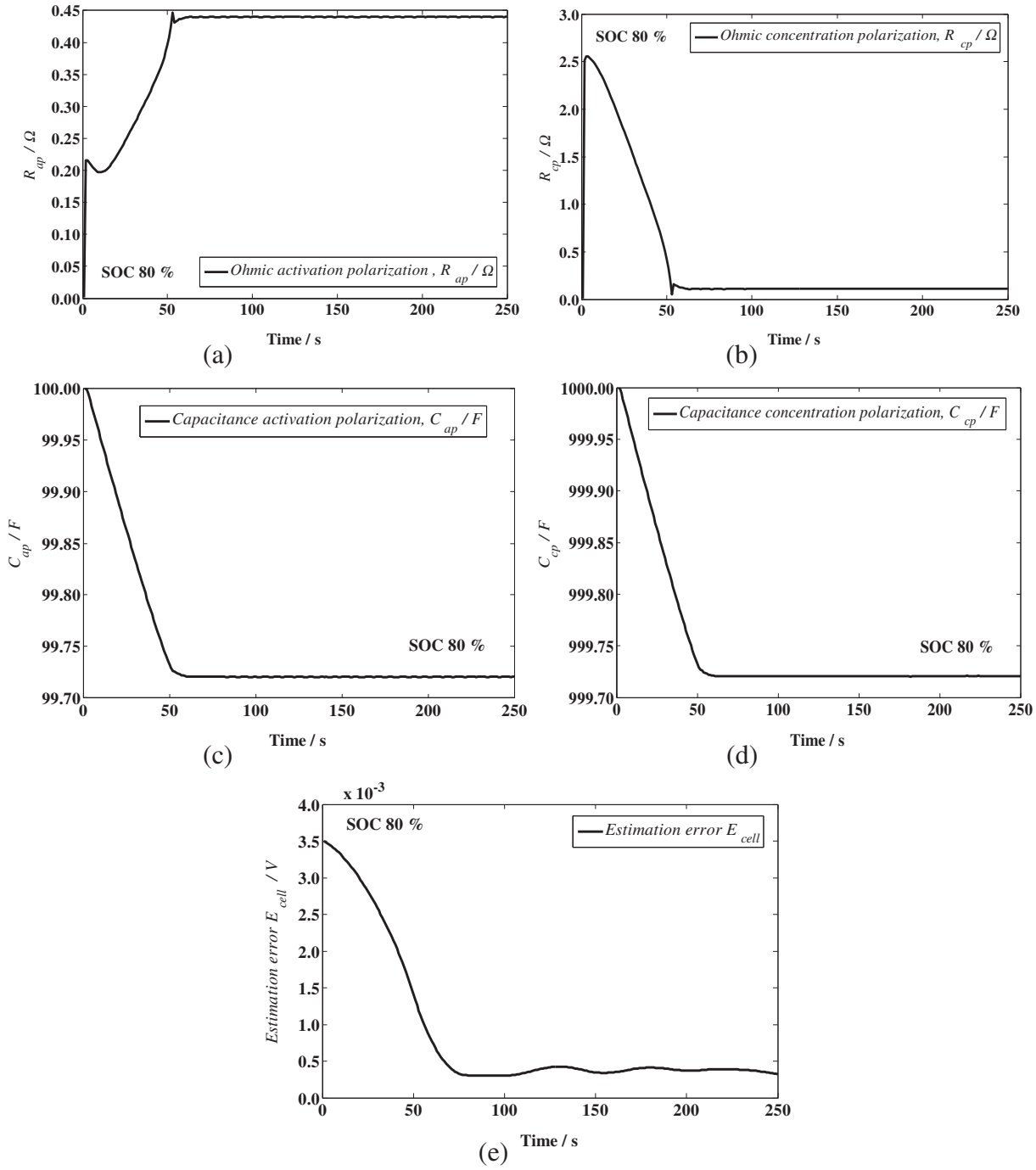

Fig. 12. Identification parameters of the V-RFB based on the implemented EKF model *vs*. time s (a) Ohmic activation polarization, (b) Ohmic concentration polarization, (c) Capacitance activation polarization, (d) Capacitance concentration polarization, and (e) Cell voltage estimation error. All data are captured at discharging mode.

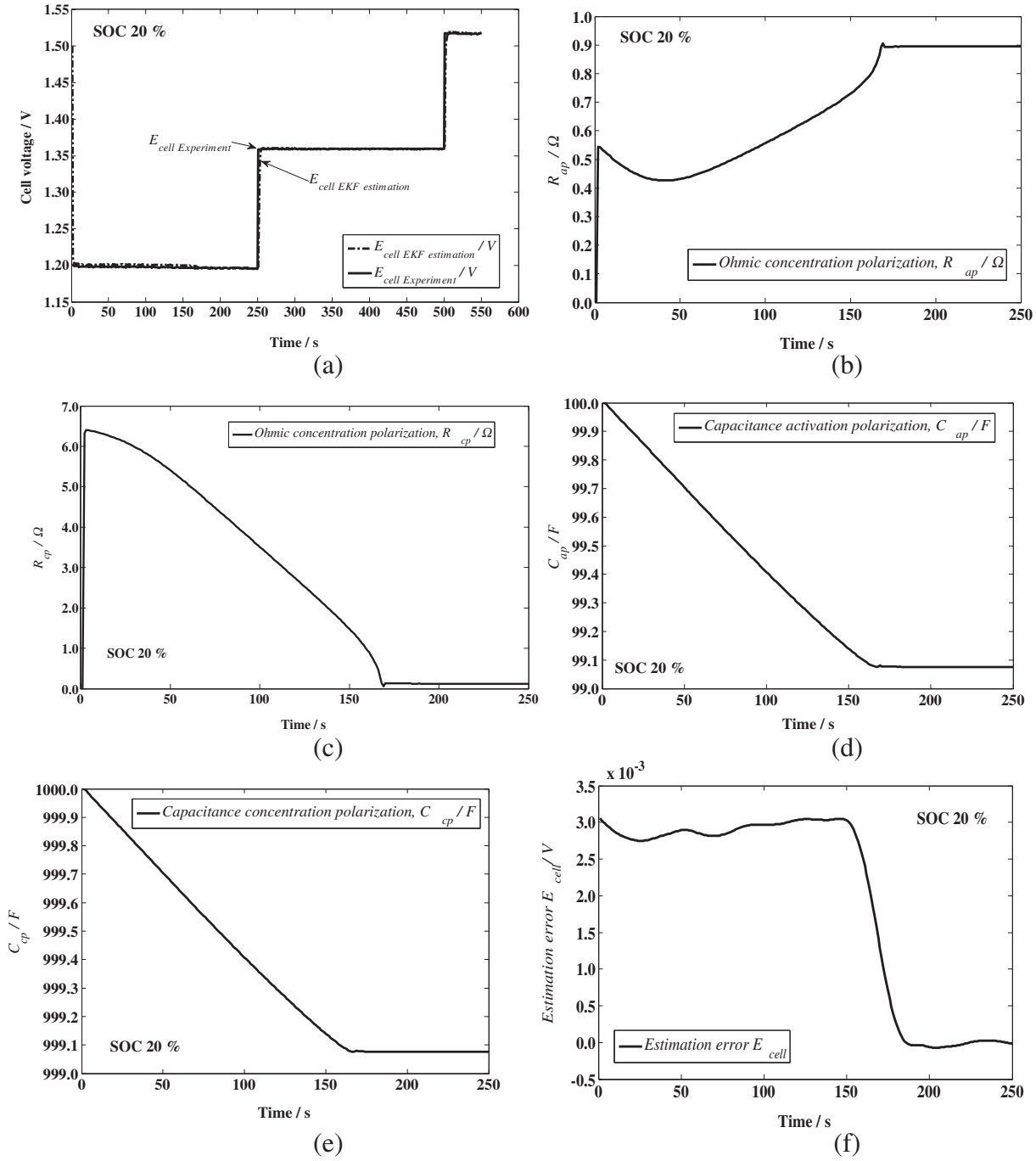

Fig. 13. Performance consistency of the tuned covariance matrix of *P*, *Q* and *R* at different SOC; 20% SOC (a) Comparison of EKF-based estimated E_{cell} and experimental E_{cell} *vs.* time of the V-RFB during pulse-relaxation test at 20% SOC, (b) Ohmic activation polarization, (c) Ohmic concentration polarization, (d) Capacitance activation polarization, (e) Capacitance concentration polarization, and (f) Cell voltage estimation error. All data, except (a), are captured at discharging mode.

The V-RFB has been discharged with a constant current of 1.5 A (corresponding to current density of 60 mA cm^{-2}) during $0 < t < 50$ s, and is followed by open-circuit period (relaxation mode) at $50 < t < 100$ s. Then, from $100 < t < 115$, the V-RFB is recharged at a constant current of 1.5 A, with each discharging mode and relaxation mode periods being delayed up to 50 s. As for the discharging mode at $0 < t < 50$ s, the delay period is needed to observe the dynamic characteristic of the V-RFB at different SOCs. Meanwhile, during the relaxation mode at $50 < t < 100$ s, the delay to is needed to ensure that the V-RFB has stabilised and recovered the unavailability capacity. On the other hand, since a constant current of 1.5 A is applied during the charge and discharge cycles, it is found that the dynamic of the V-RFB during recharge cycle is inversely proportional to battery's dynamic during discharge cycle, thus, 15 s delay are used.

The instantaneous IR_o drop during the pulse-relaxation test is given by:

$$IR_o\text{drop} = \left|E_{\text{cell},0} - E_{\text{cell},1}\right| \tag{17}$$

Hence, the ohmic resistance can be expressed as:

Table 1
EKF-based identification model parameters for a 25 cm^2 V-RFB. Operating parameters are the same as in Fig. 6.

SOC	$E_{cell\ -discharge\ starts}$/V	$t_{steady\text{-}state\ starts}$/s	R_{ap}/Ω	R_{cp}/Ω	C_{ap}/F	C_{cp}/F	Mean-error/mV
SOC20[a]	1.200	170	0.9	0.1	99.1	999.1	0.83
SOC40	1.270	110	0.78	1.2	98.5	998.5	3.5
SOC60	1.304	85	0.75	1.5	98.4	998.4	3.6
SOC80	1.348	55	0.44	0.15	99.72	999.72	2.8
Ch-Dis[b]	1.499	15	2.2	6.5	101.8	1001.8	4.9

[a] SOC20 refers to 20% SOC and so on.
[b] Ch-Dis refers to complete charge-discharge characteristic of V-RFB.

$$R_o = \frac{|E_{cell,0} - E_{cell,1}|}{|I|} \tag{18}$$

where I is the charge/discharge current of the V-RFB.

For the purpose of this study, the pulse-relaxation test is conducted on the 25 cm^{-2} unit cell, laboratory unit V-RFB at different SOCs. The V-RFB cell voltage characteristic during pulse-relaxation test at the different SOC is illustrated in Fig. 7. It should be noted that both SOC0.1 and SOC0.9 (0.1 and 0.9 represent SOC 10% and 90% respectively) overlaps each other as these are the limitations of the charge–discharge profile of the V-RFB. No relaxation mode – recharge mode are made for both SOC0.1 and SOC0.9 as these are fixed as the upper and lower limits in order to overcome the effects of side-reaction.

Based on the analysis of V-RFB cell voltage characteristic during pulse-relaxation in Fig. 7, the ohmic resistance of V-RFB as a function of SOC is shown in Fig. 8. It is observed that the ohmic resistance is independent of the charge–discharge current of the V-RFB, but varies noticeably in accordance to SOC of V-RFB. To simplify the model, the average R_o of 8.61 mΩ is used to estimate the dynamic parameters of V-RFB.

4.3. Dynamic V-RFB parameters identification

Fig. 9 demonstrates a comparison of EKF-based estimated E_{cell} and experimental E_{cell} for the 25 cm^2 unit cell, laboratory unit V-RFB during pulse-relaxation test at 80% SOC. It is observed that only minor differences exist between the EKF-based estimation and experimental results, which clearly indicates that the developed model is capable of capturing the correct qualitative trends with the fitting parameters. The ability of the model to estimate cell voltage of V-RFB as indicated by a very small mean-error of 2.8 mV is presented in Fig. 10. Nonetheless, it should be noted that the two bumps in Fig. 10 is the result of the transition mode during the pulse-relaxation test. Fig. 11 exhibits the degree of uncertainties of the state covariance which demonstrates all state estimations approaching steady state at the end of pulse-relaxation test, hence reflecting the performance and accuracy of the corresponding estimated state vector.

In this estimation stage, the covariance matrix i.e. initial state covariance, P, process noise covariance, Q and measurement noise covariance, R are tuned at:

$$\begin{aligned} P &= \mathrm{diag}\left[6e^{-2} \quad 7e^{-9} \quad 1e^{-2} \quad 1 \quad 2e^{-6} \quad 1 \quad 1e^{-10}\right] \\ Q &= \mathrm{diag}\left[1e^{-4} \quad 1e^{-4} \quad 1e^{-4} \quad 0 \quad 0 \quad 0 \quad 0\right] \\ \text{and} \quad R &= 1e^{-5} \end{aligned} \tag{19}$$

the estimated characterisation of V-RFB dynamic parameters based on EKF-based identification method during the discharge mode is shown in Fig. 12.

4.4. Model verification and validation

Consistency is an important criterion in evaluating the performance of any filter as the state estimation covariance matrix

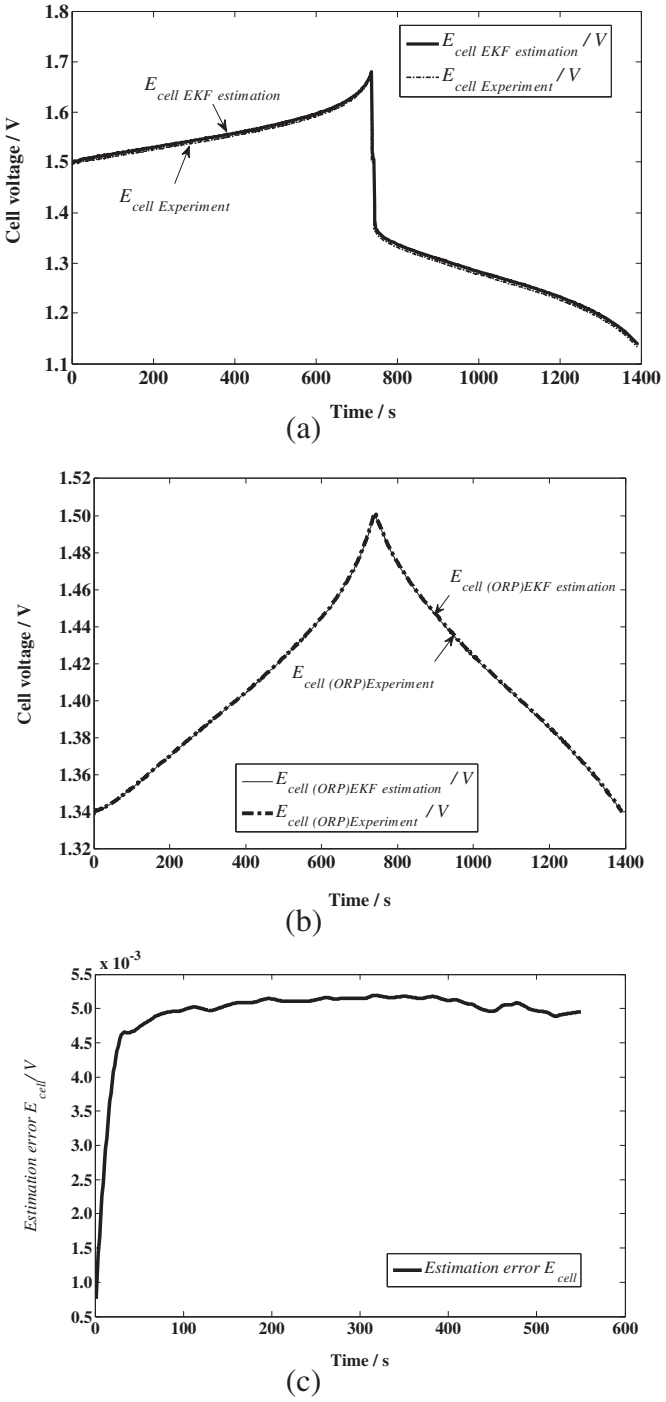

Fig. 14. Validation of EKF-based estimation model with respect to the experimental data *vs*. time (a) comparison of the E_{cell} EKF-based estimation and E_{cell} experiment, (b) comparison of the $E_{cell(ORP)}$ EKF-based estimation and $E_{cell(ORP)}$ experiment, and (c) mean-error of the EKF-based estimation with respect to the experimental data. Operating parameters are the same as in Fig. 6.

established by a filter reflects the accuracy of the state estimated vector. Therefore, to verify the consistency of the estimation covariance matrix, the tuned covariance matrix of P, Q and R are applied to different pulse-relaxation tests at different SOC. The consistency of the estimation covariance matrix in estimating the V-RFB parameters at 20% SOC is presented in Fig. 13. For simplicity of this paper, only data at 20% SOC are shown, whereas Table 1 summarises the identification parameters.

From Fig. 13, it is interesting to note that the tuned covariance matrix of P, Q and R prove to be consistent in estimating the experimental E_{cell} with mean-error recorded at 0.83 mV as well as in identifying the V-RFB's dynamic parameters. The duration required for the model to reach steady-state for convergence reduces as the SOC decreases. It is also found that the ohmic activation polarization R_{ap} reduces as the SOC level increases; a clear indication that the charge transfer resistance is dominant at lower SOC. Conversely, the concentration polarization is dominant at mid-section of SOC, showing that the cell is under mass transport control, and reduces at higher SOC as the cell is no longer under mass transport control. Also, the ohmic activation polarization is found to be always smaller than that of the concentration polarization; this indicates that, at mass-transport control, the activation polarisation affects the performance of V-RFB for a shorter period compared to that of the concentration polarisation. Similarly, it is noted that capacitance concentration polarizations are always 10 times larger than capacitance activation polarizations.

Furthermore, the mean-error is found to be in the range of mV throughout all the SOC levels, where the lowest value is noted at 20% SOC testing data but a longer duration is required to reach the convergence point.

To further demonstrate the applicability and evaluate the consistency of the model in estimating V-RFB parameters, the model has been tested on full cycle of charge–discharge characteristic of the V-RFB at the same operating parameters. Fig. 14 depicts the performance of the model in estimating both the E_{cell} and $E_{cell(ORP)}$ of the V-RFB. It is noted that the results of the EKF-based estimation model overlaps the both E_{cell} and $E_{cell(ORP)}$ throughout the charge–discharge characterization of the V-RFB with a recorded mean-error of 4.9 mV. This suggests the consistency of the model in estimating the parameters of V-RFB.

5. Conclusions

A circuit-based equivalent electrical model has been proposed for a unit cell V-RFB. Supported by the experimentally gathered V-RFB's equilibrium cell voltage and ohmic resistance, the V-RFB's dynamic parameters, which reflect the battery's polarization characteristics, are identified using the EKF algorithm. The model demonstrates to be consistent over different pulse-relaxation tests at different SOC of the V-RFB, which reflects the accuracy of the state estimated vector. Comparisons between the simulation results and experimental data have demonstrated a good degree of accuracy in predicting the trends observed in experimental test with minimum mean-error of 4.9 mV, with respect to cell voltage and open-circuit cell potential. The current model is independent of the variation in current density, flow rates, temperatures and electrolytes concentrations. The primary aim, however, is to capture the electrochemical trends within the V-RFB and represent in terms of electrical characteristics. All effects of the different operating parameters will be considered in a forthcoming paper.

Acknowledgement

This work was supported by The Malaysian Ministry of Higher Education (MOHE) and Universiti Malaysia Pahang (UMP), Malaysia. The authors are grateful to Re-Fuel Technology Ltd, UK (now RedT) for providing the equipment. Special appreciation is noted to Prof. Walsh, Dr. Sharkh and P. Ridley for the discussions on V-RFB. All experiments were carried-out at the Electrochemical Engineering Laboratory, University of Southampton, UK. On-going experiment at UMP is supported by UMP under grant RDU1203104.

References

[1] D.A.J. Rand, R.M. Dell, Journal of Power Sources 144 (2005) 568–578.
[2] N. Tokuda, T. Kanno, T. Hara, T. Shigematsu, Y. Tsutsui, A. Ikeuchi, T. Itou, T. Kumamoto, SEI Technical Review June 2000, No. 50, 2000, pp. 88–94.
[3] P.S. Fedkiw, R.W. Watts, Journal of The Electrochemical Society 131 (1984) 701–709.
[4] B. Li, L. Li, W. Wang, Z. Nie, B. Chen, X. Wei, Q. Luo, Z. Yang, V. Sprenkle, Journal of Power Sources 229 (2013) 1–5.
[5] W. Wang, Q. Luo, B. Li, X. Wei, L. Li, Z. Yang, Advanced Functional Materials 23 (2013) 970–986.
[6] C. Blanc, A. Rufer, IEEE International Conference on Sustainable Energy Technologies, ICSET2008, IEEE, Singapore, 2008, pp. 696–701.
[7] H. Al-Fetlawi, A.A. Shah, F.C. Walsh, Electrochimica Acta 55 (2009) 78–89.
[8] D. You, H. Zhang, J. Chen, Electrochimica Acta 54 (2009) 6827–6836.
[9] A.A. Shah, H. Al-Fetlawi, F.C. Walsh, Electrochimica Acta 55 (2010) 1125–1139.
[10] H. Al-Fetlawi, A.A. Shah, F.C. Walsh, Electrochimica Acta 55 (2010) 3192–3205.
[11] J. Chen, S. Zhu, B. Wang, J. Yang, Huagong Xuebao/CIESC Journal 61 (2009) 211–215.
[12] M.H. Li, T. Funaki, T. Hikihara, in: Power Conversion Conference – Nagoya, 2007. PCC'07, 2007, pp. 221–225.
[13] A.A. Shah, M.J. Watt-Smith, F.C. Walsh, Electrochimica Acta 53 (2008) 8087–8100.
[14] S. Abu-Sharkh, D. Doerffel, Journal of Power Sources 130 (2004) 266–274.
[15] D.W. Dees, V.S. Battaglia, A. Bélanger, Journal of Power Sources 110 (2002) 310–320.
[16] M. Rychcik, M. Skyllas-Kazacos, Journal of Power Sources 22 (1988) 59–67.
[17] M.R. Mohamed, S.M. Sharkh, F.C. Walsh, The 5th International IEEE Vehicle Power and Propulsion Conference (VPPC'09), IEEE, Dearborn, Michigan, 2009, pp. 551–557.
[18] Y. Hu, S. Yurkovich, Y. Guezennec, R. Bornatico, in: American Control Conference, 2008 (2008), pp. 318–325.
[19] O. Tremblay, L.-A. Dessaint, A.-I. Dekkiche, in: IEEE Vehicle Power and Propulsion Conference VPPC, 2007 (2007), pp. 284–289.
[20] J. Chahwan, C. Abbey, G. Joos, in: IEEE Canada Electrical Power Conference EPC, 2007 (2007), pp. 387–392.
[21] L. Barote, C. Marinescu, M. Georgescu, in: PowerTech, 2009 IEEE Bucharest (2009), pp. 1–6.
[22] M.R. Mohamed, H. Ahmad, M.N. Abu Seman, International Review of Electrical Engineering (IREE) 7 (2012) 5610–5622.
[23] M. Dürr, A. Cruden, S. Gair, J.R. McDonald, Journal of Power Sources 161 (2006) 1400–1411.
[24] Y. Hu, S. Yurkovich, Y. Guezennec, B.J. Yurkovich, Control Engineering Practice 17 (2009) 1190–1201.
[25] C.P. Zhang, J.Z. Liu, S.M. Sharkh, C.N. Zhang, in: International Symposium on Electric Vehicles (ISEV) (2010), p. 11. Beijing, China.
[26] H. He, X. Zhang, R. Xiong, Y. Xu, H. Guo, Energy 39 (2012) 310–318.
[27] H. Zhang, M.Y. Chow, in: 2010 IEEE Power and Energy Society General Meeting IEEE (2010), pp. 1–6. Minneapolis.
[28] H. He, R. Xiong, X. Zhang, F. Sun, J. Fan, IEEE Transactions on Vehicular Technology 60 (2011) 1461–1469.
[29] M.R. Mohamed, S.M. Sharkh, H. Ahmad, M.N. Abu Seman, F.C. Walsh, International Journal of the Physical Sciences 7 (2012) 1010–1024.
[30] M.R. Mohamed, H. Ahmad, M.N. Abu Seman, Elektronika Ir Elektrotechnika 19 (2013) 37–42.
[31] B. Ge, W. Wang, D. Bi, C.B. Rogers, F.Z. Peng, A.T. de Almeida, H. Abu-Rub, International Journal of Electrical Power & Energy Systems 44 (2013) 115–122.
[32] M. Skyllas-Kazacos, C. Menictas, in: 19th International Telecommunications Energy Conference INTELEC 97 (1997), pp. 463–471.
[33] L.T. Lam, H. Ozgun, O.V. Lim, J.A. Hamilton, L.H. Vu, D.G. Vella, D.A.J. Rand, Journal of Power Sources 53 (1995) 215–228.